

Anisotropic Stiffness Adhesives for High Shear Forces on Soft Substrates

Peter van Assenbergh,* Frank Haring, Joshua A. Dijksman, and Dimitra Dodou

Reversible attachment on soft substrates is useful in a range of applications, including soft robotics and soft-tissue surgical instrumentation. On rigid substrates, the use of micropatterned adhesives has been extensively explored. It has been shown that surface micropatterns provide conformability, thereby enabling the formation and preservation of contact with the substrate. On soft, deformable substrates, on the other hand, surface micropatterns largely lose their functionality. Alternative mechanisms have to be explored to maximize conformability and thus formation and preservation of contact on soft substrates. 3D-printing is used to fabricate adhesives with internal cylindrical pores of various configurations leading to different combinations of high/low normal/shearing stiffness, and shear forces are measured on glass and on soft elastomeric substrates. On the glass substrate, shear forces are highest for the adhesives with the lowest normal stiffness, independently from their shear stiffness. On the soft substrates, the highest shear forces are achieved for the adhesives combining low normal stiffness, enabling contact formation, with high shear stiffness, promoting contact preservation. The beneficial effect of such anisotropic stiffness on shear forces increased with the deformability of the substrate.

requires two phenomena to take place: contact formation between the adhesive and the substrate and preservation of the formed contact when external loads are applied.^[5,6] Consequently, for strong, yet reversible attachment, an adhesive should fulfil two contradictory properties simultaneously: high deformability in the normal direction, leading to a large contact formation, and low deformability in the loading direction, leading to preservation of the formed contact when loads are applied.^[7] The presence of such direction-dependent stiffness in a material is commonly referred to as “anisotropic stiffness”.^[8,9]

Dry adhesives are typically patterned with repetitive microscale elements such as pillars, spatulas, or mushrooms.^[10–14] Alternatively, patterning adhesives with wrinkles has been proposed for controlling attachment.^[15–17] When attaching to hard substrates, such surface (micro)patterns are associated with high adaptability to the substrate roughness and low effective

1. Introduction

1.1. Patterned Adhesives


Temporary attachment to substrates is useful in a range of applications, such as robotic devices performing pick-and-place tasks, climbing robots, biomedical applications such as skin patches, and fastening products on tilted or vertical substrates.^[1–4] Successful attachment of an adhesive on a substrate

requires two phenomena to take place: contact formation between the adhesive and the substrate and preservation of the formed contact when external loads are applied.^[5,11,18] Additionally, surface micropatterns allow for a more uniform stress distribution than unpatterned adhesives, which contributes to better preservation of the formed contact.^[5,6,11,18] Furthermore, the contact of surface micropatterns with the substrate is split up into multiple contact points. When locally a contact point detaches, the stress is globally rebalanced over the remaining contact points, inhibiting the propagation of the defect.^[6,11,18,19] Additionally, contact split-up in multiple smaller contacts results in a drastic increase of contact line length, and thus higher separation strength.^[15]

On soft substrates, surface micropatterns might be expected to lose at least some of their advantageous properties of forming and preserving the contact over unpatterned surfaces. Contact formation between a soft substrate and an adhesive is likely to be primarily promoted by the substrate's deformability, and so the presence of a surface micropattern might not be particularly contributing to contact formation compared to an unpatterned surface. For the preservation of contact between a soft substrate and an adhesive, the presence of a surface pattern might be even disadvantageous, because the splitting up of the contact into numerous finer elements leads to a non-uniform stress distribution at the adhesive-substrate interface, with local peak forces at the perimeter of each contact point,^[20–22] which increase the risk of crack initiation under stress. Additionally, as Cheung et al. showed, on soft polyurethane substrates with a thickness

P. van Assenbergh, F. Haring, Dr. D. Dodou
Department of Biomechanical Engineering
Faculty of Mechanical, Maritime and Materials Engineering
Delft University of Technology
Mekelweg 2, Delft 2628CD, The Netherlands
E-mail: s.p.vanassenbergh@tudelft.nl

Dr. J. A. Dijksman
Physical Chemistry and Soft Matter
Wageningen University & Research
Stippeneng 4, Wageningen 6708WE, The Netherlands

 The ORCID identification number(s) for the author(s) of this article can be found under <https://doi.org/10.1002/admi.202001173>.

© 2020 The Authors. Published by Wiley-VCH GmbH. This is an open access article under the terms of the Creative Commons Attribution License, which permits use, distribution and reproduction in any medium, provided the original work is properly cited.

DOI: 10.1002/admi.202001173

larger than 2 mm, the detachment of individual microscale cylindrical pillars led to local redistribution of stresses among neighboring pillars.^[23] Therefore, detachment of a single pillar induced detachment of the neighboring pillars and subsequent propagation of the defect throughout the whole adhesive.

1.2. Internal Geometry

Beside the surface pattern of adhesives, also the internal properties of the adhesive can be designed to realize the anisotropic properties required for good grip. For example, Bartlett et al. fabricated elastomeric adhesive pads, and internally reinforced them by incorporating stiff carbon fibres, aligned with the shear direction.^[7] The presence of these fibres resulted in a drastic increase in generated shear forces compared to elastomeric pads without reinforcement, because the low stiffness in the normal direction allowed for high contact formation, and the high stiffness in the shear direction enabled efficient preservation of contact under shear loading. Micropillar reinforcement by incorporating directional stiff fibers,^[24] or by embedding hard nanoparticles in micropillars^[25] has been also shown to prevent deformations that may cause loss of contact.

Anisotropic properties in materials have also been realized without implementation of a second, reinforcing component. For example, Tramsen et al. encased granules in an elastic membrane, and showed that high friction forces are generated due to conformation of the elastic membrane to substrate irregularities, and stiffening of the adhesive due to jamming of the granular component under normal loads.^[26] Alternatively, the presence of a flat terminal layer topping a microstructure has been shown to benefit the shear performance of adhesives on hard substrates. He et al. fabricated micropillar arrays topped with a terminal layer, and attributed the higher shear forces found compared to micropillar arrays without a terminal layer to energy loss due to elastic deformations of both the sub-surface structures and the terminal layer during peeling off, reattachment of the terminal layer during sliding, and internal sliding of the sub-surface structures along each other.^[27] The presence of multiple peeling fronts when applying load in the normal or shearing direction has been also suggested to result in a drastic increase of the peeling line length, and therefore in higher pull-off or shear forces.^[28,29]

In earlier work, we showed that, on soft substrates, micropatterned adhesives consisting of arrays of closely-packed spherical dimples, topped with a terminal layer generate higher shear forces than unpatterned adhesives as well adhesive with the same dimple micropattern but without a terminal layer.^[30] It is likely that the presence of a terminal layer results in contact formation similar to that of an unpatterned adhesive of the same dimensions. Additionally, the low stiffness of the thin terminal layer in the normal direction in combination with the high shear stiffness from the internal cavity walls allows for contact preservation during sliding.^[27,28,30] These results suggest that anisotropic stiffness enabled by a combination of an internal spherical cavity with a thin, deformable terminal layer can be beneficial for generating high shear forces.

An easy method to fabricate structures with internal geometry is 3D printing. 3D printing has been used to fabricate porous structures with anisotropic properties.^[31–34] Such anisotropic

materials are applied as, for example, porous template scaffolds for tissue engineering.^[35,36] In such scaffolds, porosity has a function to maximize permeability (which is crucial for cell growth and transport of nutrients and metabolic waste), but also to match the scaffold mechanical properties with those at the implantation site.^[35,37] Duoss et al. independently varied the shear and normal stiffness of elastomeric structures by 3D printing porous architectures consisting of stacked rasters of long filaments with diameters of 100–610 μm .^[38]

Here, we use 3D printing to fabricate adhesives with porosity-induced anisotropy and use their architecture to obtain mechanical properties suitable for generating grip on hard and soft substrates. Anisotropic properties were realized by 3D printing adhesives containing internal horizontal cylindrical pores to control the stiffness in shear and normal direction. The samples were 3D-printed from a single material. We measured shear forces of 3D printed anisotropic adhesives with different architectures, resulting in various stiffness degrees, in the shear and normal direction. Shear forces were measured on rigid glass substrates as well as on deformable poly-dimethoxysiloxane (PDMS) substrates.

2. Results

2.1. Fabricated Adhesives

2.1.1. Fabrication

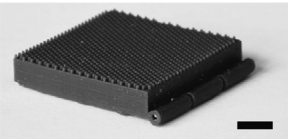

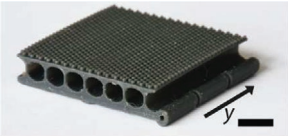

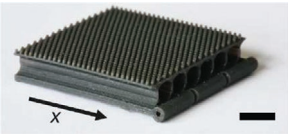


Table 1 shows the internal and external geometry of the four sample types fabricated using stereolithographic processing. The adhesives were $20 \times 20 \times 5 \text{ mm}^3$ in size (length \times width \times height) and contained either a single row of cylindrical pores of 2.7 mm in diameter separated by pore walls with a 0.5 mm thickness at their thinnest position, or a double row of pores of 1.28 mm in diameter separated by pore walls with a 0.15 mm thickness at their thinnest position. The adhesives with a single and double row of pores contained overhangs of 2.7 and 1.275 mm, respectively. Two types of adhesives with a single row of pores were fabricated: one with pores aligned parallel to the pulling direction x (SR-X) and another with pores aligned orthogonally to the pulling direction (SR-Y). Adhesives with a double row of pores were fabricated with pores aligned orthogonally to the pulling direction (DR-Y). Isotropic adhesives, without an internal geometry, were fabricated as reference samples (REF).

The four internal geometries were combined with three types of external (surface) geometries: unpatterned (UNP), a pattern of circular posts with a diameter of 0.5 mm and a height of 0.5 mm (PIL), and a pattern of conical pillars with a diameter of 0.5 mm at the base and 0.2 mm at the top, tilted 45° in x -direction (HKS).

2.1.2. Mechanical Characterization

Figure 1 shows the adhesives with four different internal geometries, without any loading (top picture), with a normal load of 6 N (middle picture) applied via a cylindrical weight and with

Table 1. Photographs of 3D-printed adhesives with different internal geometries. In shear force measurements, samples were placed on the substrate with the surface pattern facing down, and pulled in the x-direction. Scale bar of internal geometries = 5 mm; scale bar of surface patterns = 1 mm.

Internal geometries		Surface patterns	
REF No internal pores		UNP Unpatterned	
SR-Y Single row of 2.7 mm diameter cylindrical pores, aligned orthogonally to the pulling direction x		PIL Circular pillars with a diameter of 0.5 mm and a height of 0.5 mm	
SR-X Single row of 2.7 mm diameter cylindrical pores, aligned parallel to the pulling direction x		HKS Conical pillars with a diameter of 0.5 mm at the base and 0.2 mm at the top, tilted 45° in x-direction	
DR-Y Double row of 1.275 mm in diameter cylindrical pores, aligned orthogonally to the pulling direction x			

a shear load of 6 N (bottom picture). For each internal geometry, the structural stresses under an applied shear load of 6 N, as predicted by Finite Element Analysis (FEA), are shown. In FEA, we fixated the contact surface of the adhesives, so shear deformations occur in the bulk of the adhesives. In Table 2, the corresponding deformations of the adhesives under the applied loads, both in shear and normal direction, are reported.

FEA predicted that the adhesive with internal geometry REF distributes stresses throughout the bulk without local stress concentration. Experimental shear loading of this adhesive confirmed that it had the highest shear stiffness out of the four internal geometries.

For geometry SR-Y, FEA predicted that, under a shear force of 6 N, stresses in the internal walls are high. As it can be seen in Figure 1, the terminal layer experiences lower stresses in

the shear direction. Stress concentrations in the terminal layer are present underneath the internal pore walls. Shear loading of geometry SR-Y resulted in a shear deformation of 1.5 mm, caused by lateral tilting of the internal pore walls (Figure 1). Loading this geometry in the normal direction led to bending of the pore walls into an s-shape.

For geometry SR-X, FEA showed that lateral deformations under a shear force of 6 N are limited to 0.17 mm. In the terminal layer, longitudinally shaped stress concentrations were predicted, located underneath the pore walls. The corresponding empirical data showed that this geometry had the same normal stiffness but higher shear stiffness than the SR-Y geometry (Table 2).

For geometry DR-Y, FEA predicted that internal stress concentrations occur in the pore walls and are the highest closer

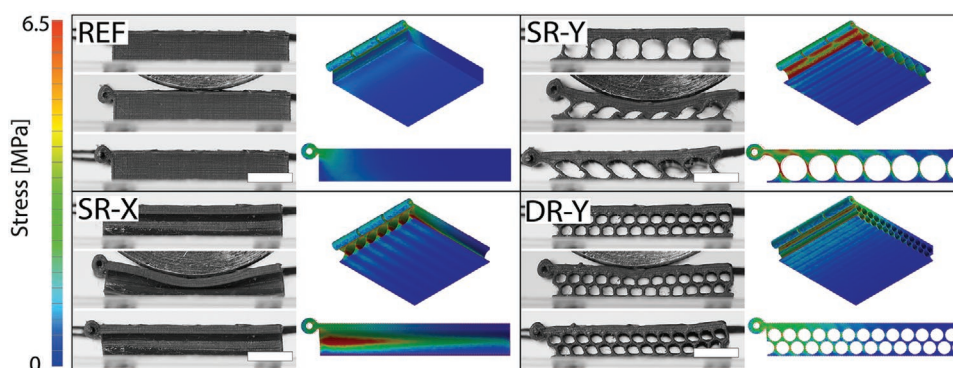


Figure 1. Adhesives with four internal geometries under no load, normal load, and shear load (from top to bottom), and stresses calculated with Finite Element Analysis (FEA) in bottom and side view graphical representations. The geometries with a single row of pores (SR-X and SR-Y) have the lowest normal stiffness. Scale bars are 5 mm.

Table 2. Experimentally determined deformations for the four internal geometries under a load of 6 N in normal and shear direction and corresponding calculated compliance k of the geometries.

	Normal direction		Shear direction	
	Deformation [mm]	k_{normal} [kN m ⁻¹]	Deformation [mm]	k_{shear} [kN m ⁻¹]
REF	<0.1	>60	<0.1	>60
SR-Y	1.5	4	1.5	4
SR-X	1.5	4	<0.1	>60
DR-Y	0.45	13.33	0.8	7.5

to the point where the shear load is applied on the adhesive. At the adhesive surface, stress concentrations are longitudinally shaped, and aligned with the pore direction. Empirical testing of this geometry showed that the shear stiffness of this geometry was in between the shear stiffness of the two single-pore row internal geometries.

2.2. Shear Forces on a Glass Substrate

Figure 2 shows the shear forces on glass for the adhesives without external geometry (UNP) as a function of internal geometry.

A two-way ANOVA for surface pattern (UNP, PIL, and HKS) and internal geometry (REF, SR-Y, SR-X, and DR-Y) showed significant main effects for both the surface pattern, $F(2,108) = 209.09$, $p < 0.001$, and the internal geometry, $F(3,36) = 62.01$, $p < 0.001$. An interaction effect of the surface pattern with the internal geometry was also found, $F(6,108) = 110.09$, $p < 0.001$.

Post-hoc analysis per external geometry group showed that, among the UNP adhesives, internal geometries SR-X and SR-Y generated significantly higher shear forces than DR-Y and REF ($p < 0.001$). Among the PIL adhesives, all three internal geometries generated higher shear forces than REF, with SR-Y resulting in significantly higher shear forces than DR-Y

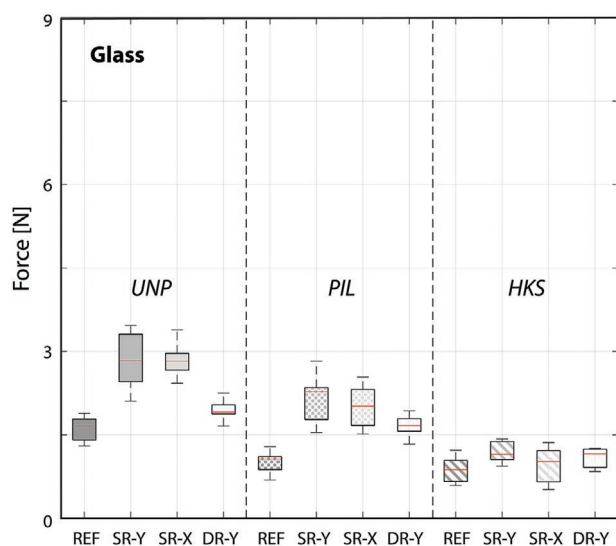


Figure 2. Shear forces of the four internal geometries, grouped by external surface pattern, on a glass substrate.

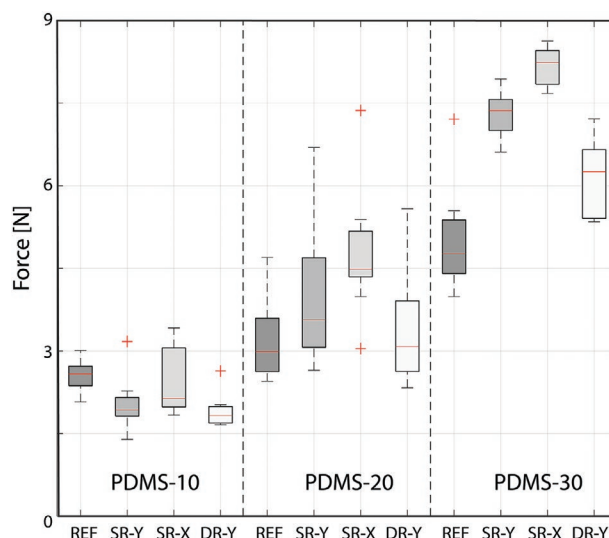


Figure 3. Shear forces of the four internal geometries and unpatterned surface geometry, grouped by PDMS substrate. The corresponding data for adhesives with surface patterns of pillars or hooks are presented in the supporting information (Figure S2, Supporting Information).

($p < 0.001$). Among the HKS adhesives, no significant differences among the four internal geometries were observed.

Post-hoc analysis per internal geometry group showed that all four internal geometries with UNP surface generated higher shear forces than the corresponding internal geometries with a HKS surface ($p < 0.001$). SR-X and SR-Y with UNP surface also generated higher shear forces than the corresponding internal geometries with surface PIL ($p < 0.001$). SR-X, SR-Y, and DR-Y with surface geometry PIL generated higher shear forces than the corresponding internal geometries with surface geometry HKS ($p < 0.001$).

2.3. Shear Forces on PDMS Substrates

Figure 3 shows the shear forces of adhesives with surface UNP as a function of internal geometry on PDMS substrates of three stiffness degrees.

A two-way ANOVA of shear forces of adhesives with surface UNP for substrate (PDMS-10, PDMS-20, and PDMS-30) and internal geometry (REF, SR-Y, SR-X, and DR-Y) showed main effects for both the substrate, $F(2, 108) = 325.7$, $p < 0.001$, and the internal geometry, $F(3,108) = 22.31$, $p < 0.001$, as well as an interaction between substrate and internal geometry, $F(6, 108) = 8.68$, $p < 0.001$.

Post-hoc analysis showed that significantly higher shear forces were generated on PDMS-30 than on PDMS-10 and PDMS-20 for all adhesives ($p < 0.001$), except for geometry REF, which did not generate significantly higher shear forces on PDMS-30 than both single-pore row adhesives on PDMS-20.

Geometries SR-X and SR-Y generated significantly higher shear forces on PDMS-20 than all four internal geometries on PDMS-10. Additionally, geometry DR-Y on PDMS-20 outperformed SR-Y and DR-Y on PDMS-10, and geometry REF on PDMS-20 outperformed DR-Y on PDMS-10 ($p < 0.001$).

On PDMS-10, no significant differences in shear forces were observed between the four internal geometries of adhesives. On PDMS-20 substrates, SR-X outperformed DR-Y and REF ($p < 0.001$). On PDMS-30, SR-X, SR-Y, and DR-Y outperformed REF, and both single-row geometries (SR-X and SR-Y) generating significantly higher shear forces than DR-Y ($p < 0.001$).

On all three PDMS substrates, adhesives with PIL and HKS surface patterns generated lower shear forces compared to adhesives with UNP surface within each of the four groups of internal geometries ($p \leq 0.003$). Furthermore, adhesives with surface HKS were outperformed by adhesives with surface PIL ($p < 0.001$). Shear forces of adhesives with surface patterns PIL and HKS on PDMS-10, PDMS-20, and PDMS-30 are presented in the supporting information.

3. Discussion

Here, we used 3D printing to generate adhesives with architectures resulting in anisotropic stiffness properties to enhance gripping performance. Such anisotropic adhesives should not be confused with adhesives that generate “anisotropic friction,” which is defined as directional grip, or grip being higher in one shearing direction than in the opposite direction.^[39–43]

3.1. Anisotropic Adhesives

3.1.1. Fabrication

In Table 1, the four fabricated internal geometries and three external geometries are shown. We used 3D printing, because it is one of the few methods suitable for fabrication of overhanging features.^[44] With stereolithography, designs are printed in consecutive layers of 50 μm in thickness. We printed the adhesives in upright position (i.e., with the $5 \times 20 \text{ mm}^2$ side of the adhesive facing down). By printing the adhesives in this orientation, the mechanical stability of each cured layer is maximized, preventing printing errors that could be caused during peeling off of each cured layer from the printing bed. We fabricated adhesive with pore diameters of 1.28 mm (in DR-Y adhesives) or 2.7 mm (SR-X and SR-Y). Pore sizes were chosen because of three factors. First, for pores below 1 mm in diameter, uncured resin could not be washed out of the pores due to capillary forces after printing with the used commercial setup and resin. Second, the wall thickness between neighboring pores had to be thick enough to support the structure, and not spontaneously collapse. Third, planned adhesive dimensions had to be in the order of 1 cm^2 , resembling the length scale of soft robotic grippers or surgical grippers. Meeting these demands, we could fit 12 neighboring pore rows in a $2 \times 2 \text{ cm}^2$ adhesive, and manufactured alternative geometries with half the amount (i.e., six) of neighboring pores.

3.1.2. Mechanical Characterization

We applied normal and shear loads of 6 N and observed the deformations of the adhesives in the corresponding loading

directions. For adhesives with a single row of pores (SR-X and SR-Y), FEA predicted that it is mainly the internal pore walls that absorb the applied stress. Under the applied normal loads, we observed that pore walls took an s-shaped when buckling. In other words, normal loading, besides deformation, also led to lateral deformation. FEA also predicted that, along the surface of the adhesive, stress concentrations are present along the pores, where the terminal layer is not supported, as the surface layer thickness is lowest on these locations.

Adhesives with internal geometries SR-Y and DR-Y showed larger deformation in the shearing direction than adhesives with SR-X internal geometry. Deformation of the adhesives mostly originated from bending of the pore walls when these are aligned with the shearing direction γ (Table 1). When pore walls are aligned with the shearing direction, as is the case in adhesives with an SR-X geometry, walls cannot deform in the direction of their alignment. Comparing a double or a single row of pores, a higher shear stiffness of DR-Y geometries compared to SR-Y adhesives originated from a lower aspect ratio and a higher accumulative length of the internal pore walls for the first geometry, reducing the bendability of the internal pore walls. Adhesives with internal geometry REF did not exhibit observable deformations under the applied shear and normal loads. The isotropic nature of this adhesive resulted in the highest geometric density of the four fabricated internal geometries, making it the stiffest adhesive. The stiffness of this adhesives is best-described by the resin's bulk tensile strength as provided by the resin manufacturer (7.7–8.5 MPa after post-curing).

3.2. Shear Forces

3.2.1. On Glass

On a glass substrate, we found that adhesives with internal pores generated higher shear forces compared to UNP adhesives, and that higher shear forces are generated with adhesives with a single row of pores then with a double row of pores. The difference in shear stiffness of internal geometries SR-X versus SR-Y did not lead to significantly different shear forces. In SR-X adhesives, bending of the pore walls is present, but this bending did not lead to deformation of the terminal layer and its subsequent detachment from the substrate. One effect that we observed was that the variation of generated shear forces was lower for higher shear stiffness adhesives (i.e., with internal geometry SR-X) compared to adhesives with internal geometry SR-Y, pointing towards an advantage in terms of performance reliability of higher shear stiffness adhesives.

In Figure 4, bottom view images of adhesives with a UNP surface and various internal geometries are shown under a preload (PL) of 2.45 N (250 g) and under the measuring load of 0.49 N (50 g) during shearing at $t = 0$ (t_0). Additional frames of video recordings are shown in the Supporting Information. The formed contact between the adhesives and the glass substrate, appearing as light regions in the bottom view, consisted of segregated contact regions. Under the applied pre-loading, the contact points of the porous internal geometries were a vertical projection of the internal pore geometry. For adhesives

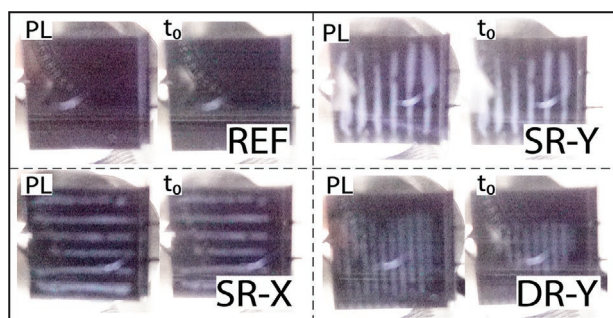


Figure 4. Bottom view of adhesives with the four internal geometries on glass under a preload (PL) of 2.45 N and at t_0 , where, about 3 s prior to sliding, the load was reduced to 0.49 N. Contact regions appear as light regions, whereas dark regions are not in contact with the substrate.

with a single row of pores (SR-X, SR-Y), the thickness of contact regions were higher compared to adhesives with a double row of pores (DR-Y), suggesting that more intimate contact was formed in the former two cases. Additionally, adhesives with a single row of pores preserved more contact after the normal load was reduced to 0.49 N. These superior contact formation and preservation properties of adhesives SR-X and SR-Y likely originated from the lower average thickness of the terminal layer, and led to higher shear forces on glass substrates compared to adhesives with a double row of pores. One could reason that the splitting-up of formed contact in multiple separated contact points, leading to inhibition of crack initiation and propagation, is higher in adhesives with a double row than in adhesives with a single row of pores. Presumably, the absence of the described effects in our adhesives is because the number of contact points is too low, and the length scale of individual contact points (contact areas are on millimeter scale) is too large for such effects to manifest themselves.

The presence of a single row of pores internal results in a 76% increase of generated shear forces on glass compared to isotropic adhesives REF, because of mentioned mechanisms.

Patterning the terminal layer with pillars (PIL) or hooks (HKS) deteriorated shear performance compared to unpatterned adhesives (REF). With the 3D printing method we used, patterns were presumably not fine enough to introduce advantageous effects of contact splitting. The spacing and the millimeter-length scale of pillars or hooks rendered a dramatic decrease in formed contact area with the substrate compared to unpatterned adhesives. A lower contact area was formed with HKS adhesives than with PIL adhesives, leading to lower shear forces. In the presence of hooks, the contact area was too low for effects of internal geometry to manifest themselves. A lower normal stiffness, introduced by bendable pore walls or terminal layers, did not compensate for the lack of contact of the HKS surface.

3.2.2. On PDMS

On soft PDMS substrates, the deformability of the substrate affected the mechanism with which shear forces are generated. Video recordings of shear force measurements of UNP adhesives on three PDMS substrates showed that the softer

the substrate is, the more contact is formed under the applied preload (**Figure 5** and Supporting Information).

We observed that, for adhesives with a UNP surface, the formation of contact was rather similar between the four internal geometries. However, the preservation of contact after reducing the load from 2.45 to 0.49 N was considerably higher in the presence of pores. Similar to results on glass substrates, contact preservation was largest for the adhesives with the lowest normal stiffness (SR-X and SR-Y).

On PDMS-10, no effect of internal geometry was found on generated shear forces. On PDMS-20 and PDMS-30, high shear stiffness combined with low normal stiffness of adhesives led to an increase of shear forces of 49% on PDMS-20 and 63% on PDMS-30. The presence of a thin terminal layer (in SR-X and SR-Y) was increasingly beneficial for the generated shear forces on substrates with decreasing stiffness compared to a relatively thicker terminal layer (as present in DR-Y). A thin terminal layer has a higher compliance, and therefore more efficiently conforms to substrate deformations, resulting in better preservation of contact under loading compared to adhesives with a thicker terminal layer.

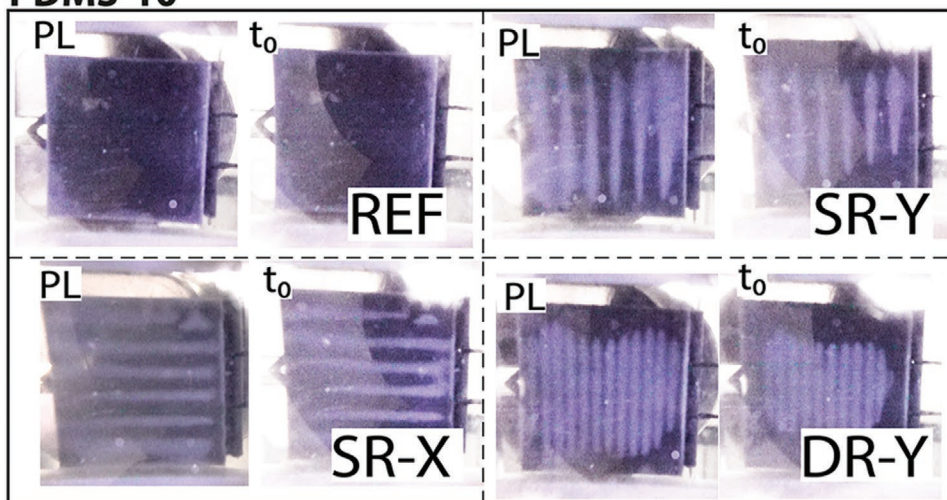
Similar to the results on glass, also on PDMS substrates, patterning the surface of adhesives with pillars (PIL) or hooks (HKS) resulted in systematically lower shear forces compared to unpatterned adhesives (UNP), likely due to reduced contact area when adhesives were patterned. As a result, effects of internal geometry were quenched when adhesives contained a patterned surface. Nevertheless, we did observe that surface patterns introduced a better distribution of contact over the adhesive-substrate interface compared to unpatterned adhesives, leading to lower stress concentrations (**Figure 6**). During sliding, the growth of defects was not continuously expanding as observed with flat adhesives, suggesting that there is less coupling between detachment of neighboring pillars or hooks. Additionally, pillars and hooks re-attached after detachment, resulting in a preservation of contact area during sliding. In the shear force measurements, these contact preservation properties were not able to compensate for the reduced total contact area with respect to unpatterned adhesives, resulting in lower shear forces. Finer surface structures (i.e., pillars or hooks with lower dimensions and spacing) might be needed to overcome the loss of contact area in patterned adhesives.

3.3. Outlook

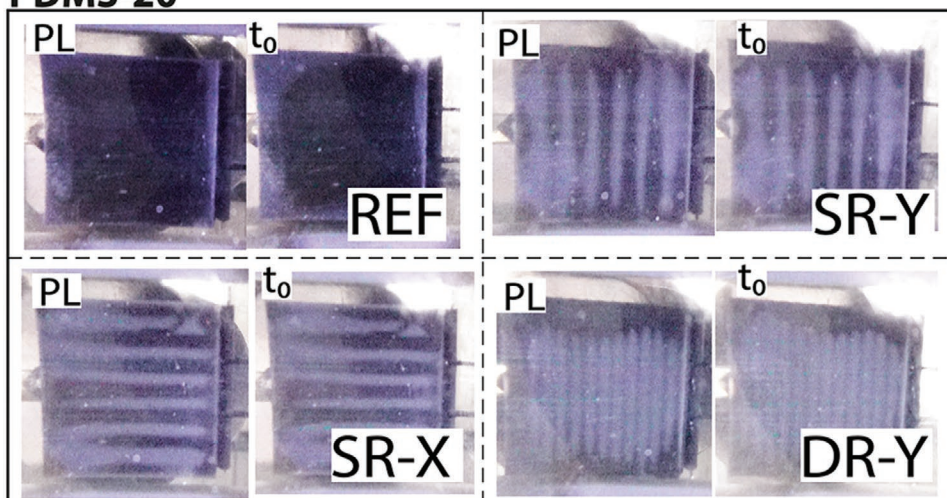
We showed that porous structures can be used to generate materials with direction-dependent stiffness. We varied pore size and pore wall thickness but one could also vary other parameters such as the shape of the pores and the overall porosity.^[32] With the structural variety that is offered by 3D printing, this approach could be extended to generate stiffness gradients in materials to improve the internal stress distribution when loads are applied. Furthermore, one could introduce unique stiffness profiles in additional directions of the adhesives, for example to realize high shear forces in the x -direction, but facilitate easy detachment in the y -direction, by lateral sliding.

The functionality of internal geometries of adhesives would benefit from higher resolutions in order to fabricate smaller

PDMS-10



PDMS-20



PDMS-30

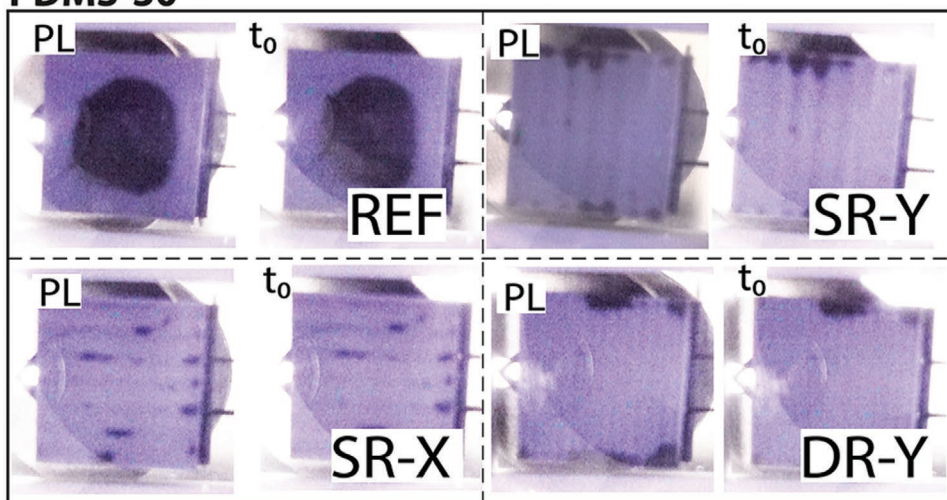


Figure 5. Contact area of adhesives with a surface UNP with various internal geometries under preload (PL) and the load applied during shearing (t_0). The light regions are those that are in contact with the substrate.

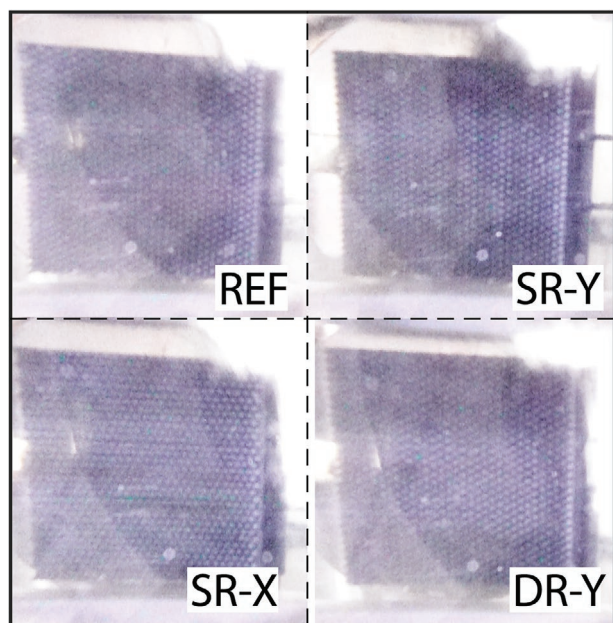


Figure 6. Effects of internal geometry of pillar adhesives on the formation of contact. Video images were recorded on PDMS20 substrates during sliding. Single-row pore geometries exhibited longitudinal close-contact regions aligned with the pore direction. A double row of pores resulted in a uniform distributed contact area in the center of the adhesive. Adhesives with intern geometry REF exhibited a large area of contact at the perimeter of the adhesive. The light regions are those that are in contact with the substrate.

features and more homogeneous stiffness. Furthermore, spatially controlling direction-dependence stiff or soft regions could be improved with smaller features such as pores and pore walls, eliminating the occurrence of local stress concentrations under loading. Smaller features will also result in thinner pore walls, making the adhesives more susceptible to fatigue after multiple times of bending and elastic recovering of the geometry. Alternative 3D printing methods deserve to be explored to obtain higher resolutions, taking into account the balance between feature size and adhesive dimensions on one side, and processing time and structural strength on the other side.^[44]

Potentially, surface patterns could be optimized for attachment to rough substrates, for example, by introducing patterns that promote interlocking,^[45,46] or for attachment to wet or flooded substrates, by introducing water-draining surface patterns.^[47] Immersion brings additional viscous dissipation and associated timescales into the mechanics of these substrates which allows for further optimization of adhesion performance.

4. Conclusion

We showed that geometry-controlled variation of normal and shear stiffness of adhesives can be used to generate reversible grip on soft, deformable substrates, as well as on rigid glass substrates. We fabricated single-material adhesives with anisotropic properties using a stereolithographic approach. We were able to fabricate adhesives with larger deformability than expected based on the reported resin stiffness. On a rigid

substrate, adhesives with the lowest normal stiffness performed best. On soft substrates, a low normal and a high shear stiffness were found to be advantageous for contact formation and preservation, respectively. In other words, decoupling of normal and shear deformations can be beneficial for contact preservation. Such anisotropy requires adhesives with rather complex adhesive architectures, which can be realized using 3D printing methods.

5. Experimental Section

Fabrication of Adhesives: Adhesives were fabricated using a Form2 printer (Formlabs inc., Somerville, MA, USA) with the suppliers recommended print settings and a layer thickness of 0.05 mm. Formlabs resin Flexible FLFLGR02 (Formlabs inc., Somerville, MA, USA) was used to fabricate $20 \times 20 \text{ mm}^2$ samples with a porous inner structure, a 0.5 mm high surface pattern and 0.4 mm solid back layer. Four types of internal geometries were printed (Table 1): The first geometry consisted of a row of 6 cylindrical pores, resulting in a pore diameter of 2.7 mm, positioned orthogonally to the pulling direction. The second geometry consisted of the same 2.7-mm diameter cylindrical pores, but now positioned parallel with the pulling direction. In the third geometry, two rows of 12 cylindrical pores, resulting in 1.275-mm diameter pores, positioned parallel to the pulling direction were fabricated. A fourth geometry was a reference sample, without any porosity. Each of these four internal geometries were fabricated either without surface pattern, with a pattern of 0.5 mm diameter circular pillars, or conical, 45° tilted pillars with a diameter of 0.5 mm at the base and 0.2 mm at the top, resulting in a total of 12 geometries. Each of these 12 adhesive types were printed twice, resulting in a total of 24 adhesives.

The printed samples were cleaned with compressed air (EW5601, Ewent, Geleen, Netherlands) and isopropyl alcohol (IPA, VWR Chemicals, Radnor, PA, USA) to remove uncured resin, and post-cured for 60 min at a temperature of 60°C in a Form Cure oven (Formlabs Inc., Somerville, MA, USA). After post-curing, the support structures were removed and the samples were kept at room temperature for 24 h to allow the IPA to fully evaporate.

Mechanical Characterization of Adhesives: Adhesives were characterized with indentation tests, performed with an Aerotech ACT115 linear motion stage, controlled with an Aerotech Soloist CP controller and a custom-built GUI in MATLAB R2016a. A FUTEK S-Beam load cell with a 10 lb capacity was mounted on the motion stage to record the forces. The load cell signal was amplified with a CPJ25 signal conditioner. The adhesives were indented using a glass lens indenter (radius of curvature = 34.5 mm, Thorlabs Inc. Newton, NJ, USA) over depth of 1.5 mm (0.5 mm for the isotropic adhesive), and forces and displacements were recorded at a frequency of 200 Hz.

FEA of Adhesives: A nonlinear static analysis was performed with Inventor Nastran2020 software (Autodesk Inc., San Rafael, CA, USA). The material model was built using the resin's mechanical properties as provided by Formlabs. The elastic modulus was derived from the shore hardness using the relations from Mix and Giacomini.^[31] A mesh was generated using the default linear elements, with an element size of 0.15 mm. The bottom of the adhesive was fixed, and a sliding constraint was applied to the central axis of the eye (where in shear force measurements, the pulling cable is connected), to ensure a pure horizontal deformation under the applied load. A bearing-load with a magnitude of 6 N was applied at the inside of the eye in the direction of pulling.

Substrate Preparation: Poly-dimethoxysiloxane (PDMS, Sylgard 184, Dow Corning, Midland, MI, USA) substrates were prepared by mixing pre-polymer and curing agent mixed in 10:1, 20:1, and 30:1 weight-based ratios, obtaining substrates of 2200, 700, and 300 kPa, respectively.^[15,23] The pre-polymer – curing agent mixtures were degassed, in measured quantities poured in 140 mm petri dishes, degassed again, and finally cured for at least 2 h at 70°C to obtain substrates of 2 mm in thickness.

A glass slide was used as glass substrate.

Shear Force Measurements: Shear force measurements were performed using a custom-made positioning stage (ACT115, Aerotech inc, Pittsburg, PA, USA) with a 9 N load cell (LSB200, FUTEK, Irvine, CA, USA), controlled with a GUI build in MATLAB R2016a. The signal from the load cell was amplified and converted with a CPJ2S signal conditioner. Samples were connected to the load cell via a HPPE Dyneema braided wire (BBVFS25, Berkley, Columbia, SC, USA). Before testing, samples were aligned by attaching an alignment weight to the rear end of the adhesive (see Figure S1 in the Supporting Information).

A 2.45 N (250 gr) normal pre-load was applied for 10 s, and a 0.49 N (50 gr) normal load during measuring, applied from 3 s before sliding. The sliding velocity was 1 mm s⁻¹, for a duration of 5 s. From the recorded force-displacement data, the peak force corresponding to the moment where the sample started sliding was extracted.

Samples were recorded in a bottom-view configuration with a webcam to monitor contact formation during preloading, and before and during sliding.

For each substrate, each adhesive sample were each measured 5 times, resulting in 10 measurements per condition.

Substrates were cleaned with ethanol every 10 measurements. PDMS substrates were replaced every 20 measurements.

Supporting Information

Supporting Information is available from the Wiley Online Library or from the author.

Acknowledgements

P.v.A. and F.H. contributed equally to this work. This research is supported by the Netherlands Organization for Scientific Research (NWO) Domain Applied and Engineering Sciences (TTW), (Open Technology Program, project 13353 "Secure and gentle grip of delicate biological tissues"). The authors kindly acknowledge Marta Scali and Paul Breedveld for their help in photographing the fabricated adhesives.

Conflict of Interest

The authors declare no Conflict of interest.

Keywords

3D-printing, anisotropic adhesives, shear forces, soft substrates

Received: July 2, 2020
Revised: September 5, 2020
Published online:

- [1] Z. Wang, Z. Wang, Z. Dai, S. Gorb, *Appl. Sci.* **2018**, 8, 114.
- [2] S. Nansai, R. Mohan, *Robotics* **2016**, 5, 14.
- [3] S. Song, C. Majidi, M. Sitti, in *IEEE Int. Conf. Intell. Robot. Syst.* **2014**.
- [4] S. Baik, H. J. Lee, D. W. Kim, J. W. Kim, Y. Lee, C. Pang, *Adv. Mater.* **2019**, 31, 1803309.
- [5] N. J. Glassmaker, A. Jagota, C. Y. Hui, J. Kim, *J. R. Soc. Interface* **2004**, 1, 23.
- [6] C.-Y. Hui, N. J. Glassmaker, T. Tang, A. Jagota, *J. R. Soc. Interface* **2004**, 1, 35.

- [7] M. D. Bartlett, A. B. Croll, D. R. King, B. M. Paret, D. J. Irschick, A. J. Crosby, *Adv. Mater.* **2012**, 24, 1078.
- [8] V. A. Gorodtsov, D. S. Lisovenko, *Mech. Mater.* **2019**, 134, 1.
- [9] R. F. S. Hearmon, *Rev. Mod. Phys.* **1946**, 18, 409.
- [10] V. Tinnemann, E. Arzt, R. Hensel, *J. Mech. Phys. Solids* **123**, 20, **2019**.
- [11] L. Heepe, S. N. Gorb, *Annu. Rev. Mater. Res.* **2014**, 44, 173.
- [12] A. Del Campo, C. Greiner, E. Arzt, *Langmuir* **2007**, 23, 10235.
- [13] L. F. Boesel, C. Cremer, E. Arzt, A. Del Campo, *Adv. Mater.* **22**, 2125, **2010**.
- [14] R. Hensel, K. Moh, E. Arzt, *Adv. Funct. Mater.* **2018**, 28, 1800865.
- [15] E. P. Chan, E. J. Smith, R. C. Hayward, A. J. Crosby, *Adv. Mater.* **2008**, 20, 711.
- [16] C. H. Lin, C. Y. Huang, J. Y. Ho, H. Y. Hsueh, *ACS Appl. Mater. Interfaces* **2020**, 12, 22365.
- [17] P. C. Lin, S. Vajpayee, A. Jagota, C. Y. Hui, S. Yang, *Soft Matter* **2008**, 4, 1830.
- [18] M. Kamperman, E. Kroner, A. del Campo, R. M. McMeeking, E. Arzt, *Adv. Eng. Mater.* **2010**, 12, 335.
- [19] R. M. McMeeking, E. Arzt, A. G. Evans, *J. Adhes.* **84**, 675, **2008**.
- [20] A. N. Gent, *Rubber Chem. Technol.* **1974**, 47, 202.
- [21] J. Y. Chung, M. K. Chaudhury, *J. Adhes.* **2005**, 81, 1119.
- [22] L. Heepe, L. Xue, S. N. Gorb, *Bio-Inspired Structured Adhesives: Biological Prototypes, Fabrication, Tribological Properties, Contact Mechanics, and Novel Concepts*, Springer, Berlin **2017**.
- [23] E. Cheung, M. Sitti, *Langmuir* **2009**, 25, 6613.
- [24] L. Xue, B. Sanz, A. Luo, K. T. Turner, X. Wang, D. Tan, R. Zhang, H. Du, M. Steinhart, C. Mijangos, M. Guttman, M. Kappl, A. Del Campo, *ACS Nano* **2017**, 11, 9711.
- [25] Y. Tian, Z. Zhao, G. Zaghi, Y. Kim, D. Zhang, R. Maboudian, *ACS Appl. Mater. Interfaces* **2015**, 7, 13232.
- [26] H. T. Tramsen, A. E. Filippov, S. N. Gorb, L. Heepe, *Adv. Mater. Interfaces* **2020**, 7, 1901930.
- [27] Z. He, C. Y. Hui, B. Levrard, Y. Bai, A. Jagota, *Sci. Rep.* **2016**, 6, 26867.
- [28] M. Varenberg, B. Murarash, Y. Kligerman, S. N. Gorb, *Appl. Phys. A Mater. Sci. Process.* **2011**, 103, 933.
- [29] K. Kendall, *J. Phys. D. Appl. Phys.* **1975**, 8, 1449.
- [30] P. van Assenbergh, M. Fokker, J. Langowski, J. van Esch, M. Kamperman, D. Dodou, *Beilstein J. Nanotechnol.* **2019**, 10, 79.
- [31] G. Alaimo, S. Marconi, L. Costato, F. Auricchio, *Compos. Part B Eng.* **2017**, 113, 371.
- [32] J. Ying, L. Lu, L. Tian, X. Yan, B. Chen, *Comput. Graph.* **2018**, 70, 157.
- [33] J. Kiendl, C. Gao, *Compos. Part B Eng.* **2020**, 180, 107562.
- [34] T. Liu, L. Liu, C. Zeng, Y. Liu, J. Leng, *Compos. Sci. Technol.* **2020**, 186, 107935.
- [35] D. J. Yoo, *Biomaterials* **2011**, 32, 7741.
- [36] F. C. Fierz, F. Beckmann, M. Huser, S. H. Irsen, B. Leukers, F. Witte, Ö. Degistirici, A. Andronache, M. Thie, B. Müller, *Biomaterials* **2008**, 29, 3799.
- [37] D. W. Huttmacher, *Biomaterials* **2000**, 21, 2529.
- [38] E. B. Duoss, T. H. Weisgraber, K. Hearon, C. Zhu, W. Small IV, T. R. Metz, J. J. Vericella, H. D. Barth, J. D. Kuntz, R. S. Maxwell, C. M. Spadaccini, T. S. Wilson, *Adv. Funct. Mater.* **2014**, 24, 4905.
- [39] J. Tamelier, S. Chary, K. L. Turner, *Langmuir* **2012**, 28, 8746.
- [40] M. P. Murphy, B. Aksak, M. Sitti, *Small* **2009**, 5, 170.
- [41] K. Jin, J. C. Cremaldi, J. S. Erickson, Y. Tian, J. N. Israelachvili, N. S. Pesika, *Adv. Funct. Mater.* **2014**, 24, 574.
- [42] M. R. Cutkosky, *Interface Focus* **2015**, 5, 20150015.
- [43] M. K. Kwak, H. E. Jeong, W. G. Bae, H. S. Jung, K. Y. Suh, *Small* **2011**, 7, 2296.
- [44] P. van Assenbergh, E. Meinders, J. Geraedts, D. Dodou, *Small* **2018**, 14, 1703401.
- [45] T. H. Büscher, S. N. Gorb, *J. Exp. Biol.* **2019**, 222, jeb209833.
- [46] S. N. Gorb, *Philos. Trans. R. Soc. A Math. Phys. Eng. Sci.* **2008**, 366, 1557.
- [47] A. Tsipenyuk, M. Varenberg, *J. R. Soc. Interface* **2014**, 11, 20140113.